Band structure of TiB_2: Orientation-dependent EELS near-edge fine structure and the effect of the core hole at the B *K* edge

K. Lie
Department of Physics, Norwegian University of Science and Technology, N-7034 Trondheim, Norway and Department of Materials, School of Process, Environmental and Materials Engineering, University of Leeds, Leeds LS2 9JT, United Kingdom

R. Brydson
Department of Materials, School of Process, Environmental and Materials Engineering, University of Leeds, LEEDS LS2 9JT, United Kingdom

H. Davock
Department of Materials Science and Engineering, University of Liverpool, Liverpool L69 3BX, United Kingdom
(Received 6 July 1998)

The ceramic compound TiB_2 has been studied by electron-energy-loss spectroscopy. Spectral shapes in the vicinity of the B *K* edge with momentum transfer $\mathbf{q}\|c$ and $\mathbf{q}\perp c$ have been investigated and compared with decomposed, calculated spectra. The dipole selection ($\Delta l=\pm 1$) rule applies, so the B *K* edge provides information on *p* final states local to boron. For a uniaxial system like TiB_2, $\mathbf{q}_\|$ is proportional to p_z and $\mathbf{q}_\perp$ is proportional to p_x+p_y. The theoretical density of states has been calculated using the *ab initio* full-potential linear augmented-plane-wave method, and, when combined with the relevant matrix elements, theoretical spectra have been obtained. While giving good agreement with experiment, our theoretical calculations show that the presence of the core hole must be considered in order to reproduce the experiments, especially for momentum transfer $\mathbf{q}_\|$ due to reduced screening in this direction. In this study the core-hole effect is calculated within the $Z+1$ supercell approximation. From the interpretation of the spectral features common hybridized electronic states between boron *p* and titanium *d* bands are observed, and the structure is highly anisotropic due to more delocalized σ bonding within the boron planes. [S0163-1829(99)02207-9]

I. INTRODUCTION

TiB_2 is a covalently bonded, brittle ceramic with several unique properties, among which are its high melting point, hardness, chemical stability, and metallic properties. It is a layered, hexagonal structure ($P6/mmm$) with hexagonal sheets of titanium and boron atoms arranged perpendicular to the *c* direction. Compared to other ceramics, TiB_2 has very high thermal and electrical conductivities. Due to its unique set of properties, TiB_2 together with other transition-metal diborides (AlB_2-type), have attracted many experimental and theoretical studies (see, e.g., Refs. 1 and 2), and have been proposed for use in a wide variety of applications. Dispersions of TiB_2 precipitates in ceramics and metals (composites) are known to improve the fracture strength and toughness in these materials,[3] and TiB_2 is also used for grain refinement in aluminum alloys.[4] TiB_2 coatings are hard and relatively inert and suitable for biomaterial applications. Furthermore, in the electrolysis of aluminum, it has been proposed to replace the carbon cathode with a TiB_2-carbon composite, and it is also an attractive material for use in cutting and extrusion tools.[5]

Electron-energy-loss spectroscopy (EELS) is an established technique for investigating the unoccupied electronic states in solids.[6] The fine structure in the region of the core edges can roughly be divided into two parts. Strong oscillations up to ~ 30 eV above threshold, called electron-energy-loss near-edge structure (ELNES) and weaker oscillations from 30 eV up to several hundred eV above the edge often designated as extended-energy-loss fine structure. EELS provides information on unoccupied electronic states and is thus equivalent to x-ray-absorption spectroscopy (XAS). In XAS, the polarization vector of incident electromagnetic radiation selects the direction probed within the crystal, whereas in EELS the momentum transfer $\mathbf{q}$ selects the direction. The momentum transfer is determined by the difference between the incoming and the scattered high-energy electrons, and may be decomposed into components parallel and perpendicular to the incident beam, as seen in Fig. 1. The advantage of EELS over XAS, however, relies on the fact that in using a transmission electron microscope to obtain the EELS spectra, extremely high spatial resolution can be obtained.

Orientation dependency in EELS arises because of the directionality of the density of unoccupied electronic states, and hence transitions to these unoccupied final states. At a given energy loss the direction of the momentum transfer changes rapidly from parallel to perpendicular to the beam as the scattering angle increases. For a parallel beam of incident electrons the crossover in the weighting of the two components occurs at about $8\theta_E$, where $\theta_E=E/2\gamma T$ (the denominator here being twice the relativistic corrected kinetic energy of the incoming electrons).[7] If the collection angle is small then principally $\mathbf{q}_\|$ is sampled during an EELS experiment conducted with the crystal in a given orientation; otherwise scattering events over a wide range of $\mathbf{q}$ vectors are

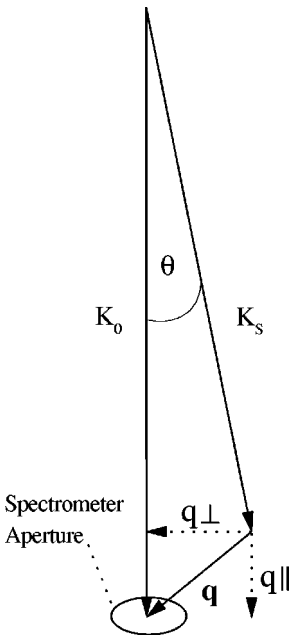

FIG. 1. Momentum-transfer components for a fast electron undergoing inelastic scattering.

collected. In the case of isotropic materials the spectra are not influenced by the direction of the momentum transfer relative to the beam. For anisotropic materials, however, the situation is different. Orientation-dependent energy loss measurements have been recorded previously for anisotropic structures such as graphite, boron nitride, and high-T_c superconductors.[7–9] In the early work of Leapman, Fejes, and Silcox[8] in their study of BN and graphite, they used a parallel electron beam incident on a specimen with the *c* axis at an angle of 45°, and obtained the two components separately. The basic structure of graphite consists of σ bonding between the C atoms perpendicular to the *c* axes and the π bonds parallel to the *c* axes. When the momentum transfer is parallel to the *c* axes, states of π character are greatly enhanced over those with σ character, whereas if the vector is perpendicular to the *c* axes the reverse is true. Their results obtained for BN and graphite showed excellent agreement with theory. Browning, Yuan, and Brown[7] proposed an alternative approach in order to retrieve the two components. The near-edge structures seen at a given orientation, are compared for small and large axial collection angles. The different approaches for retrieving momentum-dependent energy loss measurements were recently reviewed by Botton, Boothroyd, and Stobbs.[10]

Anisotropic effects were observed earlier in TiB_2/Al multilayers.[11] The motivation for the present work is to improve our understanding of the experimental data, and relate this to the electronic structure, which is closely connected to the physical properties. We report the observations of orientation dependent ELNES at the B *K* edge of TiB_2 at 188 eV. Experimental conditions were such that the dipole approximation is satisfied; therefore in the ELNES region we are probing $2p$ final states local to the boron site. In order to resolve the momentum-transfer components we used a small axial collection angle, and acquired spectra along different crystallographic orientations. The experimental spectra have been compared with theoretically determined spectra, calculated using the full-potential linear augmented-plane-wave (FLAPW) method.[12]

II. EXPERIMENTAL CONSIDERATIONS

EEL spectra were collected using a parallel recording Gatan 666 spectrometer fitted to a Phillips CM 20 transmission electron microscope (LaB_6 source), operating at a nominal voltage of 200 kV. The spectra were obtained with an energy dispersion of 0.1 eV/channel, convergence angle $\alpha = 3.0$ mrad, and a collection angle $\beta = 1.5$ mrad. The B *K* edges were acquired in diffraction mode (image coupling) with a 100-μm condenser aperture. The energy resolution (measured as the full width at half maximum at the zero loss peak) was typically around 1.8 eV. With the parameters listed above, the characteristic angle θ_E was 0.7 mrad. In this situation the collection angle is about $2\theta_E$, and is small compared to the crossover in the weighting of the two components, which occurs at about $8\theta_E$. This implies that there is good resolution of the two components, and that the momentum transfer parallel to the beam is the dominant factor. For the experimental conditions there is a convergent beam ($\alpha = 3$ mrad), but for small scattering angles the relationship between the two components is only slightly modified.[7] The processing of the sintered TiB_2 ceramic is described elsewhere;[1] however, the polycrystalline nature of the sample permits a large range of specimen orientations to be studied with limited tilting. Thin specimens were prepared by low-angle ion milling, and energy-loss measurements were carried out soon after thin foil preparation to minimize any possible oxidation effects.

Spectra from areas showing negligible oxygen contents and of similar thickness ($t/\lambda = 0.6$), as measured relative to the total inelastic mean free path of the 200-keV electrons, were compared when the orientation dependency was analyzed. The absolute energy scale was referenced to the first peak in the TiB_2 B *K* ELNES which was set to 188.6 eV as observed in isostructural CrB_2.[13] Spectra were acquired parallel and normal to the *c* axes together with the zone [2423] which is about 64° off the *c* direction. Further spectra were acquired near but not exactly on the zone. When near edge features were analyzed, however, no significant channelling effects could be detected. Spectra were deconvoluted using the Fourier-ratio method, as the low loss contribution was measured separately.

The dark current due to the photodiode array was subtracted from the spectra. Gain variations were corrected for by acquiring several spectra (8) at different positions on the photodiode array, and averaging them to produce a gain corrected spectrum as described by Boothroyd, Sato, and Yamada.[14] This approach permits the use of a shorter integration time (1 s), which is required to improve energy resolution, while still having a good signal-to-noise ratio. The continuum background before the edge was fitted and subtracted using the standard power-law procedure.

III. THEORY AND CALCULATIONS

The theoretical calculations are based on the local-density approximation within density functional theory, and use of the FLAPW method to solve the Kohn-Sham equation[15] self-

consistently. Similar to the linear-muffin-tin-orbital (LMTO) approach, the unit cell of the solid is divided up into muffin tin spheres centered on the atomic sites, and an interstitial region; however, one unique feature of the FLAPW calculations is that no shape approximation is made to the potential or charge density: no spherical average of the potential is assumed within the muffin tins spheres and, in the interstitial region, no volume average is taken as in the LMTO approach. The program package given by Blaha *et al.*[12] is used. In this study we used 126 irreducible Brillouin-zone k points for the primitive cell and 27 irreducible k points for the supercell. For both cells angular momenta $l_{max}=12$ and muffin-tin radius for the atomic species (Ti and B) were chosen equal to 2.0 a.u. and 1.6 a.u. respectively. Furthermore, 381 logarithmic mesh points inside the muffin-tin radius were used and a product of $R_{MT}K_{MAX}$ equal to 9 was obtained.

Electron-energy-loss near-edge structure provides information about the unoccupied part of the band above the Fermi energy (E_F). The differential cross section for scattering as derived from Fermi's golden rule,[16] is, within the dipole approximation, proportional to

$$\frac{d\sigma}{dE} \propto \{|m_{L+1}|^2\rho_{L+1}(E)+|m_{L-1}|^2\rho_{L-1}(E)\}, \qquad (1)$$

$$m_{L\pm1}=\langle f_{L\pm1}|r|i_L\rangle.$$

Here ρ is the density of unoccupied states with angular momentum $L\pm1$, $|i\rangle$ represents the initial inner-shell electron wave function, and $|f\rangle$ represents the final unoccupied state.

It can be seen from Eq. (1) that the near-edge structure (NES) can be related to the local angular-momentum-resolved density of states (DOS) projected onto the atomic site in question. This means that a K $(1s)$ shell excitation provides information about the unoccupied p DOS. More specifically in uniaxial systems $\mathbf{q}\perp c$ is proportional to p_x+p_y, while $\mathbf{q}\|c$ is proportional to p_z. Because the initial wave function $|i\rangle$ is a well-defined atomic wave function, the challenge of calculating the NES lies in calculating the final-state wave function $|f\rangle$. The augmented-plane-wave approach uses products of radial wave functions and spherical harmonics inside the muffin tins, and expands the wave function in the space between the muffin tins as plane waves. This band structure method only gives you the ground state, and does not include correlations caused by the excitation process (e.g., core-hole effect). The core-hole effect arises from the incomplete screening of the nuclear charge as an electron is excited from a localized core state. Physically, the excited atom can be thought of as an impurity in the material, with an associated local distortion of the electronic structure (and no atomic relaxation during the time scale of the excitation). In the absence of screening, the core hole may be approximated as an extra nuclear charge at the excited atomic site—this is commonly known as the $Z+1$ approximation. In the present work the core hole was approximated by performing a supercell calculation in which there is a single excited $Z+1$ potential in each cell. The supercell consisted of 24 atoms ($2\times2\times2$ primitive cell), and was large enough to avoid interaction between neighboring excited potentials in different cells. In principle the supercell should be increased in size until the spectra converge.

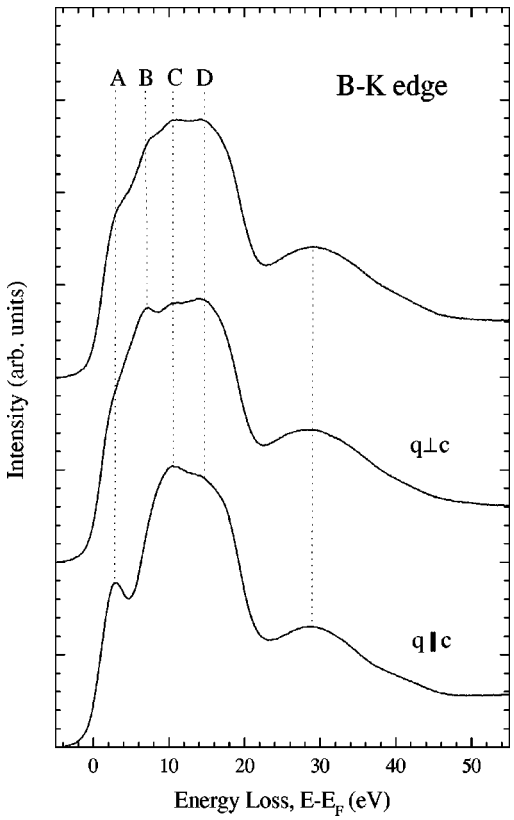

FIG. 2. Experimental B K-edge spectra along three different directions $\mathbf{q}\|c$, $\mathbf{q}\perp c$, and $\mathbf{q}\|[2423]$. Spectra are shifted and scaled for comparison.

IV. RESULTS AND DISCUSSION

As demonstrated in Secs. I and II, the normal axial method can give momentum-dependent energy-loss information. We therefore applied this technique to study TiB_2 parallel and normal to the boron planes. Figure 2 shows the near-edge structure of the B K edge for $\mathbf{q}\perp c$, $\mathbf{q}\|c$, and $\mathbf{q}\|[2423]$ obtained with a small aperture centered around the primary beam. For $\mathbf{q}\|c$ the peak A at 3.0 eV is enhanced, while peak B at 7.2 eV is enhanced for $\mathbf{q}\perp c$. Significantly, spectra acquired under these conditions exhibit strong anisotropy parallel and normal to the layers. Furthermore the spectra exhibits peaks C and D at 10.5 and 14.5 eV respectively. Both features are present in both spectra, but the peak D is slightly more pronounced for $\mathbf{q}\perp c$. In the case of $\mathbf{q}\|[2423]$ the near-edge structure is similar to an average of the spectra parallel and normal to the c axes. It shows all the features mentioned above, but the peaks are somewhat smeared out. This spectrum should be proportional to the total B p density of states.

The anisotropy presented above is in good agreement with our theoretical spectra, and we now consider the relation between the energy-loss spectrum and the electronic structure of TiB_2. The main features of the total occupied Ti and B DOS have been reported previously.[2] The total DOS profiles of TiB_2 with the FLAPW method (shown in Fig. 3) agree with these previous calculations using the LMTO-ASA

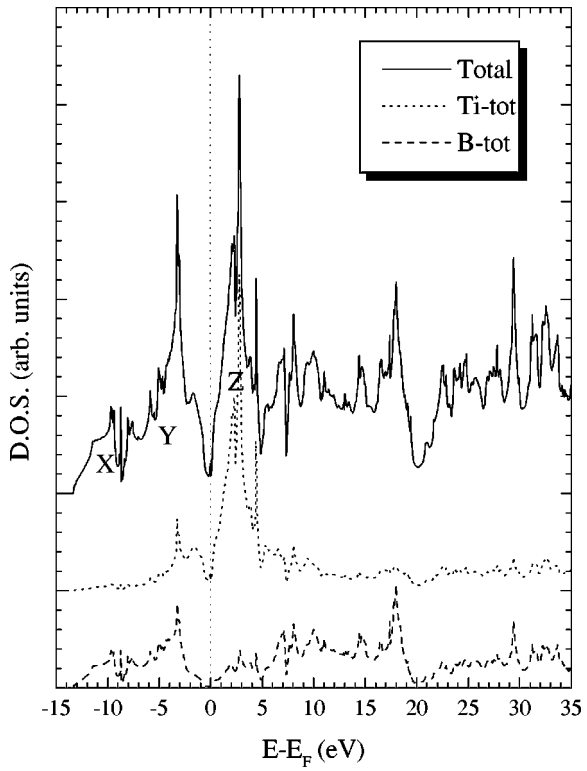

FIG. 3. Density of states in TiB_2, showing the total DOS, and the contributions decomposed at the Ti and B sites. The profiles have been shifted vertically on the intensity scale.

technique. The main features of the total DOS were assigned, with increasing energy, by Tian and Wang;[2] peak *X* is essentially due to the boron $2s$ states, the broad peak *Y* corresponds to the boron $2p$ and titanium $3d$ states, and the sharp peak *Z* just above the Fermi level is related to the nonbonding titanium $3d$ states. They also pointed out a pronounced mixing between the Ti $3d$ and B $2p$ states over a wide range from the bottom of the valence band up to E_F. Other authors, using different computational techniques such as Korringa-Kohn-Rostoker for CrB_2[17] and the APW method for ZrB_2,[18] also reported the same general features for the total occupied DOS. A ''pseudogap'' separating the bonding and nonbonding states is well defined in our DOS, and is located exactly at the Fermi level. A decomposition of the total DOS onto the Ti and B sites also reveals the hybridization in the region 0–5 eV above E_F (Fig. 3). This is important to notice considering that with EELS we are probing unoccupied electronic states.

In Fig. 4 we represent straightforward calculations of the $1s \rightarrow 2p$ transitions within the perfectly screened approximation (no core hole) resolved into $p_x + p_y$ and p_z components. Compared with features *A*–*D* in Fig. 2, there is an excellent correspondence between the peak positions in the energy-loss spectrum and the corresponding partial density of unoccupied states (see Table I). The relative intensity of the peaks also show an excellent agreement for $\mathbf{q} \perp c$; for $\mathbf{q} \| c$, however, the agreement is not totally satisfactory. The peak at 18 eV is too intense in the calculations compared with the experimental data, especially for the p_z component. The reason for this behavior will be discussed below. We obtained similar, although less accurate, results using non-self-consistent cluster-based multiple-scattering calculations.[16]

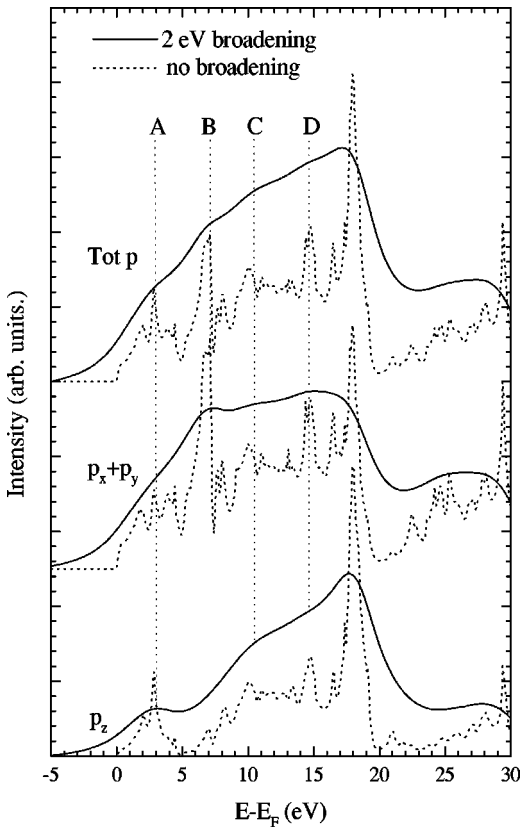

FIG. 4. Theoretical decomposed *K*-edge spectra of boron in TiB_2 within the sudden approximation—-no core-hole effects. For the solid line a 2-eV Lorentzian broadening is applied to the calculated results, and spectra are shifted and scaled for comparison.

TiB_2 consists of hexagonal sheets of B atoms perpendicular to the *c* direction that are sandwiched between layers of Ti atoms. The σ^* peak at 7.2 eV, seen most strongly in $\mathbf{q} \perp c$, results from the in-plane sp^2 hybrids in the hexagonal B sheets. This type of bonding is not present between the sheets, and the structure is highly anisotropic which is reflected in the spectral properties. The feature at 3 eV, present for the momentum transfer parallel to *c*, is due to hybridization, and possibly charge transfer, between the Ti *d* and B p_z states. We clearly see in Fig. 5 that the B p_z DOS reflects the Ti d DOS in the interval 0–5 eV. This leads to common electronic states between the Ti *d* and the B p_z states, arising from covalent bonding between the boron and titanium sheets. This feature at 3 eV may also be rationalized by consideration of the possible charge transfer from Ti to B, resulting in a π^* antibonding state. However, since there is a large hybridization of Ti $3d$ and B $2p$ states, it is natural to consider that charge transfer will not be so significant. Inte-

TABLE I. A comparison of experimental and calculated (ground state) peak positions. Note that the experimental peak at 3.0 eV for $\mathbf{q}_\|$ and the experimental σ^* peak at 7.2 eV for $\mathbf{q}_\perp$ have been aligned with theory.

Peak position	*A*	*B*	*C*	*D*
Experimental	3.0	7.2	10.5	14.6
Theoretical	3.0	7.2	10.5	14.7

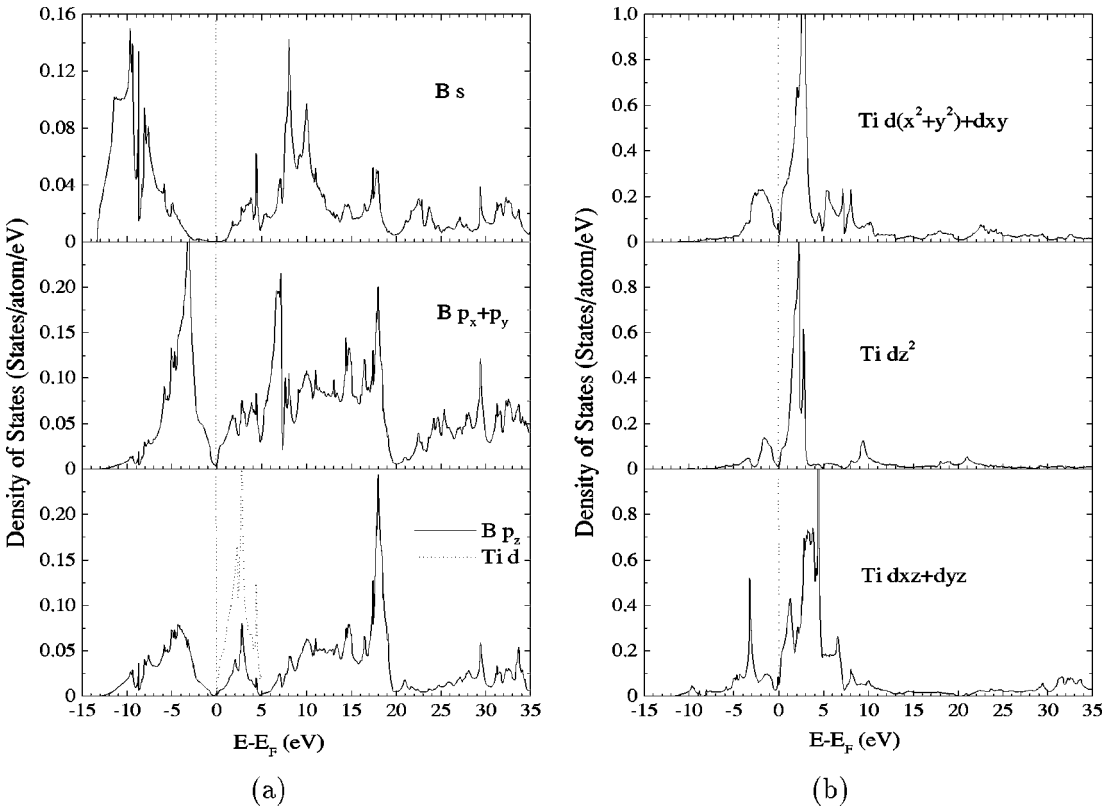

FIG. 5. Calculated symmetry-resolved (ground state) density of states in TiB_2: (a) B site showing nondegenerate partial p states and s states. Note that the total Ti d DOS is shown superimposed with the B p_z states, and is scaled for comparison. (b) Ti site showing the nondegenerate partial d states.

gration of the total B DOS indicates a charge transfer of about 0.28 electrons from Ti to B, and is consistent with previous calculated values.[2] Also experimental x-ray photoemission spectroscopy[19] and proton-induced x-ray emission[20] data suggest that almost no electron delocalization or transfer takes place in the case of TiB_2. An interesting finding in the interval 0–5 eV, shown in Fig. 5 is that, in terms of their energy position, the p_z states are strongly correlated with the total Ti d states implying a substantial degree of hybridization as stated above. The p_x+p_y states, meanwhile, essentially mix with the Ti $(d_{xz}+d_{yz})$ and d_{z^2} states. In the valence band, of all the Ti d states, it appears that the Ti $(d_{xz}+d_{yz})$ hybridize most with the out of plane (p_z) and in-plane (p_x+p_y) B p states, and that the p_z states are slightly lower in energy relative to the p_x+p_y states. These findings can be rationalized by the degree of overlap with Ti d states; since the p_z states are pointing out of the boron planes toward Ti, they will have a larger overlap integral.

As pointed out earlier, the peak at 18 eV in the calculations is too intense for the p_z component. In the experimental spectra we do not see any pronounced feature at this energy. The interpretation for this behavior is that core-hole effects in the experiment increase the spectral weight at the threshold. In this situation the relative intensity is altered. As the core electron is ejected the nuclear charge is only partially screened. This has the effect of pulling states in the conduction band down toward the Fermi level, and causing a contraction of the wave functions at the threshold.[21] Figures 6 and 7 show the calculations in both the sudden approxima-

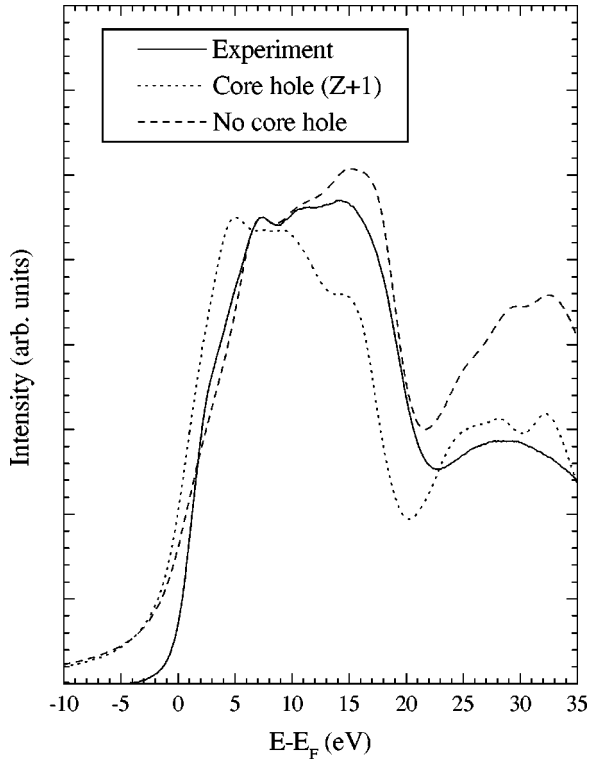

FIG. 6. Theoretical B K-edge spectra (p_x+p_y) of TiB_2—with and without the core hole, together with the experimental $(\mathbf{q}\perp c)$ spectrum for comparison. The core-hole calculations used a 24-atom supercell. The experimental data have been shifted and aligned with the spectrum in the sudden approximation at the σ^* peak at 7.2 eV.

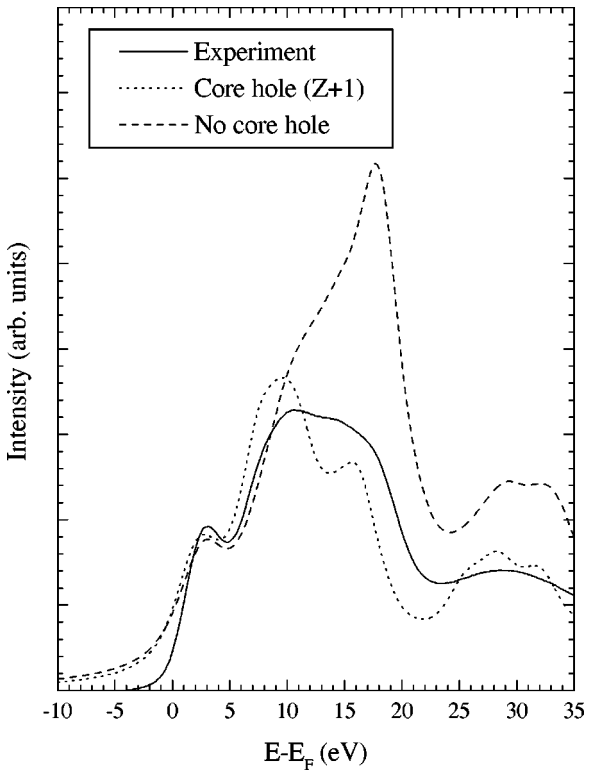

FIG. 7. Theoretical B K-edge spectra (p_z) of TiB_2—with and without the core hole, together with the experimental ($\mathbf{q}\|c$) spectrum for comparison. The core-hole calculations used a 24-atom supercell. The experimental data have been shifted and aligned with the spectrum in the sudden approximation at a peak at 3 eV.

tion and the supercell approximation for the core hole for $\mathbf{q}\perp c$ and $\mathbf{q}\|c$, respectively. In the $Z+1$ approximation the energy position of the peaks are moved down toward the Fermi level, as expected. The experimental EELS spectra are also shown for comparison. As can be seen the relative weights of the peaks for $\mathbf{q}\|c$ has significantly improved with the inclusion of the core hole. The overestimated intensity for the peak at 18 eV in the sudden approximation is reduced relative to the peaks at 3.0, 10.5, and 14.6 eV, and shows better agreement with experiment. It should also be noticed that there is a gap in the DOS at 20 eV; therefore, the 2-eV broadened spectra tend to smear out the feature at 18 eV. When we compare the calculated and experimental spectra for the two directions, it is clear that the spectrum within the boron plane is less influenced by the core hole. The reason for this behavior is that the valence electrons in the sp^2 hybrids, forming the trigonally bonded boron sheet perpendicular to c, participate in the screening of the core hole for the states within the boron planes. In other words, the bonding within this sheet has a degree of metallic character which will be reflected in the anisotropic nature of quantities such as thermal and electrical conductivity. This can be seen in Fig. 5, where the number of electrons, represented as the integral up to E_F, is larger for the p_x+p_y states relative p_z. The p_z states are also slightly more localized, which implies that the elcetrons present here have less of a screening effect. The core-hole effect is therefore more pronounced along the c direction. This also explains why the peak at 14.5 eV in the experimental spectrum for $\mathbf{q}\|c$ is less pronounced than for the data within the boron planes. The inclusion of the core-hole effects substantially improves the appearance of the calculated spectra for the momentum transfer parallel to c. This means that the nuclear charge is only partially screened along this direction and there is some excitonic modifications. The small charge transfer from Ti is not enough to screen the core hole effectively, so we may interpret the B p_z DOS in the interval 0–5 as arising from the tail of the localized d orbitals of Ti atoms.

V. CONCLUSION

Excellent agreement is found between the results of theoretical FLAPW band structure calculations and experimental ELNES for the analysis of the unoccupied electronic states of TiB_2. By performing orientation-dependent measurements and calculations it is possible to gain information about the anisotropic bonding in this material. These differences in bonding will have important consequences for anisotropic properties such as thermal and electrical conductivity. Significant improvement in the agreement between the theoretical and experimental spectrum obtained with the momentum transfer parallel the c axis (p_z) was found after the inclusion of single-particle core-hole effects, using the supercell approximation; this was found not to be the case for the spectrum with the momentum transfer perpendicular to the c axis. This is rationalized in terms of enhanced screening of the core hole for electronic transitions perpendicular to c, where the bonding has significant metallic character, and only partial screening for transitions parallel to c.

ACKNOWLEDGMENTS

The authors are grateful to the Norwegian Research Council for financial support. We acknowledge Gunnar Pettersen, NTNU, for providing the sintered TiB_2 specimen and Peter Blaha, Technical University-Wien, for help and information on the WIEN97 program.

[1] G. Pettersen, Ph.D. thesis, Norwegian University of Science and Technology, 1997.
[2] D. C. Tian and X. B. Wang, J. Phys.: Condens. Matter **4**, 8765 (1992).
[3] T. Jüngling *et al.*, Int. J. Refractory Metals Hard Mater. **12**, 71 (1994).
[4] J. D. Verhoeven, *Fundamentals of Physical Metallurgy* (Wiley, New York, 1975).
[5] J. H. Ulvensøn, Ph.D. thesis, Dept. of Metallurgy NTH, Trondheim, 1994.
[6] R. F. Egeton, *EELS in the Electron Microscope* (Plenum, New York, 1996).
[7] N. D. Browning, J. Yuan, and L. M. Brown, Ultramicroscopy **38**, 291 (1991).
[8] R. D. Leapman, P. L. Fejes, and J. Silcox, Phys. Rev. B **28**, 2361 (1983).

[9] J. Fink *et al.*, J. Electron Spectrosc. Relat. Phenom. **66**, 395 (1994).
[10] G. A. Botton, C. B. Boothroyd, and W. M. Stobbs, Ultramicroscopy **59**, 93 (1995).
[11] H. J. Davock *et al.*, in *Proceedings of EMAG97*, IOP Conf. Proc. No. 153 (Institute of Physics and Physical Society, Cambridge, 1997), Vol. 153, pp. 609–612.
[12] P. Blaha, K. Schwarz, P. Dufek, and R. Augustyn, WIEN97, Vienna University of Technology 1997. (Improved and updated Unix version of the original copyrighted Wien code, which was published by P. Blaha, K. Schwarz, P. Sorantin, and S. B. Trickey, Comput. Phys. Commun. **59**, 399 (1990).
[13] L. A. J. Garvie, A. J. Craven, and R. Brydson, Am. Mineral. **80**, 1132 (1995).
[14] C. B. Boothroyd, K. Sato, and K. Yamada, in *Proceedings of the 7th International Conference for Electron Microscopy*, edited by L. O. Peachey and D. B. Williams (San Francisco Press, San Francisco, 1990), Vol. 2, p. 80.
[15] W. Kohn and L. J. Sham, Phys. Rev. **140**, A1133 (1965).
[16] D. D. Vvedensky, in *Unoccupied Electronic States: Fundamentals of XANES, EELS, IPS and BIS*, edited by J. C. Fuggle and J. E. Inglesfield, Topics in Applied Physics Vol. 69 (Springer, Berlin, 1992).
[17] S. H. Liu, L. Kopp, W. B. England, and H. W. Myron, Phys. Rev. B **11**, 3463 (1975).
[18] H. Ihara, M. Hirabayashi, and H. Nakagawa, Phys. Rev. B **16**, 726 (1977).
[19] C. D. Wagner *et al.*, *Handbook of X-ray Photoelectron Spectroscopy* (Perkin-Elmer Corporation, Eden Prairie, MN, 1997).
[20] H. C. Padhi, C. R. Bhuinya, and B. B. Dhal, J. Phys. B **26**, 4465 (1993).
[21] R. Ahuja *et al.*, Phys. Rev. B **54**, 14 396 (1996).